

# Constraint-Guided Learning of Data-driven Health Indicator Models: An Application on the Pronostia Bearing Dataset

Yonas Tefera<sup>1,2,3,4</sup>, Quinten Van Baelen<sup>1,2,3</sup>, Maarten Meire<sup>1,2,3</sup>, Stijn Luca<sup>5</sup> and Peter Karsmakers<sup>1,2,3</sup>

<sup>1</sup> *KU Leuven, Dept. of Computer Science, ADVISE-DTAI, Kleinhofstraat 4, B-2440 Geel, Belgium*

<sup>2</sup> *Leuven.AI - KU Leuven institute for AI*

<sup>3</sup> *Flanders Make @ KU Leuven*

{*yonas.tefera, quinten.vanbaelen, maarten.meire, peter.karsmakers*}@kuleuven.be

<sup>4</sup> *Addis Ababa University, School of Electrical and Computer Engineering, Addis Ababa, Ethiopia*  
*yonas.yehualaeshet@aau.edu.et*

<sup>5</sup> *Ghent University, Department of Data Analysis and Mathematical Modelling, Coupure Links 653, 9000 Gent, Belgium*  
*stijn.luca@ugent.be*

## ABSTRACT

This paper presents a constraint-guided deep learning framework to develop physically consistent health indicators in bearing prognostics and health management. Conventional data-driven approaches often lack physical plausibility, while physics-based models are limited by incomplete knowledge of complex systems. To address this, we integrate domain knowledge into deep learning models via constraints, ensuring monotonicity, bounding output ranges between 1 and 0 (representing healthy to failed states respectively), and maintaining consistency between signal energy trends and health indicator estimates. This eliminates the need for complex loss term balancing to incorporate domain knowledge. We implement a constraint-guided gradient descent optimization within an autoencoder architecture, creating a constrained autoencoder. However, the framework is flexible and can be applied to other architectures as well. Using time-frequency representations of accelerometer signals from the Pronostia dataset, the constrained model generates more accurate and reliable representations of bearing health compared to conventional methods. It produces smoother degradation profiles that align with the expected physical behavior. Model performance is assessed using three metrics: trendability, robustness, and consistency. When compared to a conventional baseline model, the constrained model shows significant improvement in all three metrics. Another baseline incorpo-

rated the monotonicity behavior directly into the loss function using a soft-ranking approach. While this approach outperforms the constrained model in trendability, due to its explicit monotonicity enforcement, the constrained model performed better in robustness and consistency, providing stable and interpretable health indicator estimates over time. The results of the ablation study confirm that the monotonicity constraint enhances trendability, the boundary constraint ensures consistency, and the energy-health indicator consistency constraint improves robustness. These findings demonstrate the effectiveness of constraint-guided deep learning in producing reliable and physically meaningful health indicators for bearing prognostics and health management, offering a promising direction for future prognostic applications.

## 1. INTRODUCTION

Prognostics and Health Management (PHM) is a domain that focuses on the management of the health of engineering systems and their critical components. It involves monitoring an asset's condition through sensors, collecting data to assess the health status, and predicting future health by analyzing these data. This insight is then used to enhance the asset's overall reliability and availability. PHM primarily addresses three key aspects (Lei et al., 2018): the construction of Health Indicator (HI), the prediction of the Remaining Useful Life (RUL) and the management of asset health. The construction of HIs is a crucial step in assessing and predicting the condition of assets (Biggio & Kastanis, 2020). The goal is to extract effective features from sensor signals to establish stable metrics or indicators that reflect the asset's degradation

Yonas Tefera et al. This is an open-access article distributed under the terms of the Creative Commons Attribution 3.0 United States License, which permits unrestricted use, distribution, and reproduction in any medium, provided the original author and source are credited.

over time. Preferably, these indicators should have a fixed range, such as 1 to 0, where 1 represents a healthy condition and 0 indicates a faulty one. This allows for the definition of a threshold that can trigger an alarm if the HI falls below it, providing an early warning before the system escalates into critical failure.

Bearings, as vital components of machinery in various industrial applications, are subjected to high stress and wear (Cubillo, Perinpanayagam, & Esperon-Miguez, 2016). As a result, an effective PHM for bearings is vital in preventing unexpected failures, improving operational efficiency, and prolonging the service life of the machines. Consequently, it is crucial to develop efficient techniques for monitoring bearing health. Various methods are employed in the industry to monitor bearing health and detect early signs of failure (Brkovic et al., 2017). There are two main aspects that are important in these techniques (Zhou et al., 2022): (i) the detection of incipient bearing failures to avert unexpected fatal damage, and (ii) the tracking and characterization of the health condition's evolution over time.

The modeling approaches used in the construction of HIs for bearings are broadly categorized into two types: physics-based methods and data-driven methods (Li, Zhang, Li, & Si, 2024). Physics-based methods (Xu, Kohtz, Boakye, Gardoni, & Wang, 2023) involve analyzing and modeling the physical failure mechanisms of bearings using fundamental principles. When these mechanisms or relevant domain knowledge are well understood and the parameters of these physical models can be accurately estimated from measurement data, physics-based methods can provide precise, generalizable and interpretable HI values. However, in most cases, particularly for complex engineering systems, the physical failure mechanisms and domain knowledge may be incomplete or scarcely available. In this situation, the established physical models must make simplifications or assumptions, which leads to a poor representative models (Lei et al., 2016). Thus, as an alternative, data-driven methods can be applied (Jieyang et al., 2023), which are particularly promising for tackling complex processes that are not entirely understood or when physics-based methods are too computationally demanding. Data-driven methods have relatively high data collection requirements and do not require extensive consideration of the physical meaning of the data (Lu, Wang, Zhang, & Gu, 2024). Although data-driven models can achieve high accuracy in fitting observed data, they often lack physical realism or plausibility when interpolating or extrapolating beyond the available labeled data, leading to poor generalization. It is clear that both physics-based and data-driven methods have their unique strengths and weaknesses. As a result, a sensible strategy is to combine these two types of methods to take advantage of their respective merits through a hybrid approach (Liao & Köttig, 2014). Unlike the typical combination found in hybrid methods, embedding physical knowledge into

data-driven models holds promise to guide models towards generating physically consistent results (Von Rueden et al., 2023). Accordingly, there is a need to train data-driven machine learning (ML) models by incorporating physical or domain knowledge (Karniadakis et al., 2021; Meng, Seo, Cao, Griesemer, & Liu, 2022) to improve the interpretability of the model. This domain knowledge often comes in the form of physical models, constraints, dependencies, and known valid ranges of features (Muralidhar, Islam, Marwah, Karpatne, & Ramakrishnan, 2018). There are various methods to incorporate specific physical or domain information into ML models, enabling the development of robust physics-informed ML systems. These methods include physics-informed data augmentation (Xiong, Fink, Zhou, & Ma, 2023), architecture design (Nascimento & Viana, 2019; Chen & Liu, 2021), residual modeling (Willard, Jia, Xu, Steinbach, & Kumar, 2022), and modifying the loss function to include a physics-inspired regularization term (Wang, Li, Zhao, & Gao, 2020; Raissi, Perdikaris, & Karniadakis, 2019). In the latter methods, the optimization procedure is adapted such that during learning models that are not consistent with the domain knowledge are penalized to guide learning towards a model that makes a trade-off between explaining the measurements and being consistent with domain knowledge. Adding domain knowledge to learning can be considered as a regularization method which can reduce the need for labeled data, shrink the search space during model optimization, and enhance the model's generalizability to unseen scenarios (Li et al., 2024). Using this strategy, the domain knowledge described by some formal representation, such as an inequality constraint, is transferred to the parameter values of a (black box) data-driven model. In our opinion, this strategy is one of the most convenient ways to embed knowledge in data-driven models; therefore, it is selected for designing HI models in this work.

In prior works, physics-inspired constraints were considered by adding an additional regularization term to the loss function. Such a term requires a proper trade-off hyperparameter, which requires careful balancing with the other terms in the objective function. Especially when more constraints are considered, which all require their own hyperparameter, such balancing can become cumbersome. In this work, a unified framework proposed by Van Baelen and Karsmakers (2023) used to include domain knowledge in a data-driven approach to estimate the HI for bearings. This framework does not require a tuning of the hyperparameters of the different regularization terms and can be easily extended with the inclusion of additional domain-knowledge inspired constraints. More specifically, in this work the following constraints are considered: monotonicity, bounded ranges from fully healthy to failure states, and a characteristic degradation pattern informed by energy trends. This approach allows HI estimates to remain within defined ranges and adhere to the actual observed degradation patterns of a bearing, with-

out the need to rely on a predefined shape of the degradation function. The proposed method will be experimentally tested and compared with two baseline HI model learning methods using the Pronostia data set.

The remainder of this paper is organized as follows. In Section 2, we present the proposed novel methodology that discusses the training approach, the proposed constraints, and the baseline methods used. Section 3 discusses the experimental setup starting with the general HI construction procedure, description of the data set, the pre-processing procedure, the model architecture used, the data set partitioning procedure and the evaluation metrics. In Section 4, we describe the implementation of our proposed approach and discuss the results. In addition, a comparison of the results with a conventional baseline analysis is implemented. An ablation study is presented in Section 5 to discuss performance changes by slightly modifying the proposed model. Finally, in Section 6, we conclude by summarizing the results of our experiments.

## 2. METHODOLOGY

The proposed method for constructing a bearing HI model leverages domain knowledge to guide the training process, resulting in a robust and accurate model. Incorporating domain knowledge during training is expected to reduce the reliance on labeled data. Unlike other approaches in the literature, domain knowledge in this work is not integrated by adding a regularization term to the loss function. Instead, the method employs the Constraint Guided Gradient Descent (CGGD) framework proposed in (Van Baelen & Karsmakers, 2023), which facilitates solving constrained non-linear optimization problems. Specifically, this framework is utilized to train a Deep Learning (DL) model by minimizing a loss function while ensuring that the model satisfies certain constraints. These constraints represent domain knowledge. In this way, domain knowledge can be embedded into the resulting DL model. First, the application of the CGGD framework to develop DL-based HI models is described. Next, a detailed explanation of the domain-knowledge inspired constraints are provided along with their implementation within the CGGD framework. Finally, the baseline methods used for comparison with the proposed approach are explained.

### 2.1. Constraint Guided Learning of a DL based HI Model

DL architectures commonly used in PHM (Rezaeianjouybari & Shang, 2020) include Convolutional Neural Networks (CNN), Autoencoders (AE), Deep Belief Networks (DBN), Recurrent Neural Networks (RNN) and Generative Adversarial Networks (GAN). In systems where obtaining representative labeled data is challenging, the use of unsupervised learning methods, such as AE architectures, are particularly beneficial (Hoffmann Souza, da Costa, & de Oliveira

Ramos, 2023). Although the proposed method is agnostic to the model architecture and learning procedure, in this work a Convolutional Autoencoder (CAE) model architecture learned by using a reconstruction loss is adopted as a starting point. As will be explained later in Section 3, acceleration signals are transformed into a time-frequency representation denoted as  $X \in \mathbb{R}^{D \times T}$  to be used as an input to the model.

In its original formulation, the CAE model is trained to construct a compact latent representation  $z \in \mathbb{R}^{D'}$  of input signals  $X$  with  $D' \ll D$  using an encoder function  $\mathcal{E}$ . This process occurs without significant loss of information. Given  $z$ , a decoder  $\mathcal{D}$  reconstructs the input to  $\hat{X}$ , aiming to closely resemble the original signal  $X$ . During learning, the model parameters are determined using the following objective (Vincent et al., 2010):

$$\min_{\theta_{\mathcal{E}}, \theta_{\mathcal{D}}} \mathcal{L}_{\text{reconn}}(\mathbf{X}, \theta_{\mathcal{E}}, \theta_{\mathcal{D}}), \quad (1)$$

where  $\mathbf{X}$  denotes the set of all input samples,  $\mathcal{L}_{\text{reconn}}(\mathbf{X}, \theta_{\mathcal{E}}, \theta_{\mathcal{D}}) = \sum_{X \in \mathbf{X}} \|X - \mathcal{D}(\mathcal{E}(X))\|_2^2$  denotes the reconstruction loss, and  $\theta_{\mathcal{E}}$  and  $\theta_{\mathcal{D}}$  are the parameters of the encoder  $\mathcal{E}$  and decoder  $\mathcal{D}$  models, respectively. The model is trained using data segments from a healthy bearing in operation, resulting in a minimal reconstruction error for this healthy state. In contrast, in scenarios where the bearing is faulty, the reconstruction process becomes less accurate, leading to a larger reconstruction error. This increased error serves as an indicator of bearing health degradation. Once the CAE parameters are learned, the HI estimate for an input  $X$  is calculated using  $f_{\text{HI}}^{\text{CAE}}(X) = -\|X - \mathcal{D}(\mathcal{E}(X))\|_2$  which computes the reconstruction error and will have a decreasing trend over time.

Using the CGGD framework, the optimization problem provided in Eq. (1) can be turned into a constrained optimization task as:

$$\begin{aligned} \min_{\theta_{\mathcal{E}}, \theta_{\mathcal{D}}} \quad & \mathcal{L}_{\text{reconn}}(\mathbf{X}, \theta_{\mathcal{E}}, \theta_{\mathcal{D}}) \\ \text{s.t.} \quad & C_i(\mathbf{X}, \theta_{\mathcal{E}}, \theta_{\mathcal{D}}), \quad \text{for } i = 1, \dots, M. \end{aligned} \quad (2)$$

where  $C_i : \mathbb{R}^n \rightarrow \mathbb{R}$  is the  $i$ -th constraint, and  $M$  is used to denote the number of constraints incorporated in the model. To apply CGGD, a direction  $\text{dir}_{\mathbf{C}}$  needs to be defined for each constraint individually. This direction, when used to update the model, will result in a local improvement with respect to the constraint considered. For example, the constraint  $C : \mathbb{R}^2 \rightarrow \mathbb{R} : (x_1, x_2) \mapsto x_1 - x_2$  with  $C(x_1, x_2) \leq 0$  can be given a possible direction by  $\text{dir}_{\mathbf{C}} = (\frac{\sqrt{2}}{2}, -\frac{\sqrt{2}}{2})$ . Consider, for example, an intermediate solution  $(x_1, x_2) = (3, 1)$  which does not satisfy the constraint. Observe that when the gradient of a gradient descent based optimizer is replaced by the direction  $\text{dir}_{\mathbf{C}}$ ,  $(x_1, x_2) = (3, 1) - \eta(\frac{\sqrt{2}}{2}, -\frac{\sqrt{2}}{2})$ , that the updated solution, for a large enough  $\eta$ , will satisfy the constraint as  $x_1$  can be decreased and  $x_2$  can be increased until

they at least have an equal value.

To provide greater flexibility, this work employs a CGGD based CAE (CCAЕ), where the HI value is not derived from the reconstruction error, as in conventional CAEs, but is instead defined as a learnable function of the encoding  $\mathcal{E}(X)$ . This will be denoted as  $f_{\text{HI}}^{\text{CCAЕ}}(\mathcal{E}(X))$  with the learnable parameters  $\theta_{\text{HI}}$ .

## 2.2. Constraints

In this section, the constraints applied in this work are described to ensure that the predicted bearing HI values accurately reflect their degradation over time. These constraints are designed to represent domain knowledge to ultimately improve the accuracy and robustness of the model even in situations where annotated data is scarce.

### 2.2.1. Monotonic Degradation Constraint

When a bearing is put into operation, it undergoes inevitable wear, progressively worsening over time. This degradation should be reflected in the predicted HI, which is expected to decrease monotonically over time. To enforce this constraint, the HI estimates should be penalized if they deviate from the expected monotonic trend based on the time location of the corresponding input data samples. For inputs  $X_t$  measured at time step  $t$  and the corresponding health state predictions  $f_{\text{HI}}^{\text{CCAЕ}}(\mathcal{E}(X_t))$ , the monotonic degradation constraint can be expressed as follows:

For  $t_1 < t_2$ , hence  $X_{t_1}$  a measurement taken before  $X_{t_2}$  then it must hold that  $f_{\text{HI}}^{\text{CCAЕ}}(\mathcal{E}(X_{t_1})) > f_{\text{HI}}^{\text{CCAЕ}}(\mathcal{E}(X_{t_2}))$ . To enforce such a constraint with CGGD, a direction function needs to be defined, which is done by comparing the ranks of  $f_{\text{HI}}^{\text{CCAЕ}}(\mathcal{E}(X_t))$  (from high to low value) estimates with their corresponding ranks in time (from early to later). This is calculated as follows:

$$\text{dir}_{\text{mono}}(X_t, \mathbf{X}, t, \theta_{\mathcal{E}}, \theta_{\text{HI}}) = \text{rank}_{\text{desc}}(X_t, \mathbf{X}, \theta_{\mathcal{E}}, \theta_{\text{HI}}) - \text{rank}_{\text{asc}}(\text{time}(X_t), t), \quad (3)$$

where  $t$  is a set of timestamps aligned with the samples in set  $\mathbf{X}$ ,  $X_t$  is an element from set  $\mathbf{X}$ ,  $\text{time}(X_t)$  a function that extract the time at which the sample  $X_t$  was measured,  $\text{rank}_{\text{desc}}(\cdot)$  is a function that outputs the rank of  $f_{\text{HI}}^{\text{CCAЕ}}(\mathcal{E}(X_t))$  when compared to all other HI estimates of the elements in  $\mathbf{X}$  when ranked in descending order,  $\text{rank}_{\text{asc}}(\cdot)$  is a function that outputs the rank of  $t$  among all values in  $t$  sorted in ascending order.

As time progresses, it is expected that the corresponding HI estimates decrease. A positive value for  $\text{dir}_{\text{mono}}$  implies that the HI estimate is ranked too high, suggesting that a decrease in the HI estimate is necessary. In contrast, a negative value implies a lower rank, indicating that the HI estimate should be increased. A value of zero means that the HI estimate matches

its expected rank. A significant deviation in the ranking of a sample from the desired position will have a greater impact on the direction than a smaller deviation. By incorporating this monotonic degradation constraint into the HI estimation process, the model ensures that the predicted HI values decrease monotonically over time, aligning with the expected degradation pattern of the bearing.

### 2.2.2. Energy-HI Consistency Constraint

Building on the monotonic degradation constraint, we expect that while the HI values should decrease over time, the difference between the HI values of two consecutive samples should not vary significantly unless a substantial change in signal energy occurs. To enforce this concept, a constraint is introduced that ensures that if two samples have similar energy levels, their HI estimates should also be close in value.

We define this relationship mathematically as follows:

$$f_{\text{HI}}^{\text{CCAЕ}}(\mathcal{E}(X_{t_0})) - \alpha\Delta \leq f_{\text{HI}}^{\text{CCAЕ}}(\mathcal{E}(X_{t_i})) < f_{\text{HI}}^{\text{CCAЕ}}(\mathcal{E}(X_{t_0})), \quad (4)$$

where  $\Delta = \max(\kappa, |E(X_{t_i}) - E(X_{t_0})|)$  represents the normalized total energy<sup>1</sup> difference between the two samples at times  $t_0$  and  $t_i$  where  $t_i > t_0$ ,  $\alpha > 0$  is a hyperparameter that controls the sensitivity of this constraint and  $0 < \kappa < 1$ .  $\kappa$  is a parameter that introduces flexibility in the HI predictions between samples that exhibit similar energy values. Specifically, when the energy difference between the samples is minimal,  $\kappa$  allows a margin of flexibility in the HI predictions.

Based on the predicted HI of the model, the subsequent update direction of the energy-HI consistency constraint is determined as follows:

$$\text{dir}_{\text{ene}}(X_t, X_{t_0}, \theta_{\mathcal{E}}, \theta_{\text{HI}}) = \begin{cases} 1, & f_{\text{HI}}^{\text{CCAЕ}}(\mathcal{E}(X_t)) > f_{\text{HI}}^{\text{CCAЕ}}(\mathcal{E}(X_{t_0})), \\ 0, & -\alpha\Delta \leq f_{\text{HI}}^{\text{CCAЕ}}(\mathcal{E}(X_t)) - f_{\text{HI}}^{\text{CCAЕ}}(\mathcal{E}(X_{t_0})) < 0, \\ -1, & \text{otherwise.} \end{cases} \quad (5)$$

By penalizing discrepancies between the energy difference and the HI difference, we encourage the model to maintain a consistent relationship between these two variables. This approach helps prevent large fluctuations in the HI values and ensures that the model accurately reflects the gradual degradation process of the bearing.

### 2.2.3. HI Boundary Constraint

When predicting the HI of a bearing, it is convenient that the values remain within a normalized range: a fully healthy state is represented by a value of  $ub = 1$ , while a failure state corresponds to a value of  $lb = 0$ . To enforce this condition,

<sup>1</sup>The energy  $E(\cdot)$  is calculated by summing all squared elements in  $X$ .

boundary constraints are enforced during the training process to ensure that all HI predictions fall within this defined range.

In addition to the broader bound ranges, stricter bound ranges are also applied during certain phases of the bearing's life cycle. In the initial  $a\%$  (e.g.  $a = 10$ ) of its operation, the HI value is expected to be at least  $b_a < ub$  (e.g.  $b_a = 0.9$ ), ensuring that the new bearings operate in near-optimal health. In contrast, in the final  $b\%$  (e.g.  $b = 5$ ) of its operation, the HI is expected not to exceed  $b_b > lb$  (e.g.  $b_b = 0.05$ ), indicating that the bearing is close to failure due to significant degradation.

Based on the predicted HI, the subsequent upper and lower boundary constraints direction is determined as follows:

$$\text{dir}_{\text{upper}}(X_t, \theta_{\mathcal{E}}, \theta_{\text{HI}}) = \begin{cases} 1, & \text{if } f_{\text{HI}}^{\text{CCAE}}(\mathcal{E}(X_t)) > ub, \\ 0, & \text{otherwise,} \end{cases}$$

$$\text{dir}_{\text{lower}}(X_t, \theta_{\mathcal{E}}, \theta_{\text{HI}}) = \begin{cases} -1, & \text{if } f_{\text{HI}}^{\text{CCAE}}(\mathcal{E}(X_t)) < lb, \\ 0, & \text{otherwise,} \end{cases}$$

where  $lb$  and  $ub$  are the lower and upper bounds, respectively, within which the HI predictions should lie.

When  $\text{dir}_{\text{upper}}$  is 1, it means that the HI estimate is greater than  $ub$ , which requires a reduction in subsequent updates. When  $\text{dir}_{\text{lower}}$  is -1, the HI estimate is below  $lb$  and should be increased. A zero in both  $\text{dir}_{\text{upper}}$  and  $\text{dir}_{\text{lower}}$  indicates that the HI estimate is within the specified bounds and that no adjustments are necessary. By implementing these boundary constraints, it is ensured that the HI predictions accurately reflect the bearing condition, from optimal functionality to failure.

### 2.3. Implementing the Constraints in the CGGD Framework

This section provides a comprehensive explanation on how the CGGD framework can be used to train the HI estimator model, denoted as  $f_{\text{HI}}^{\text{CCAE}}(\mathcal{E}(\cdot))$ . As is indirectly indicated in Eq. (2), a multi-head network model is used. One head decodes the encoded input to calculate the reconstruction loss (to calculate  $\mathcal{L}_{\text{reconn}}$ ) and another head is used for the HI prediction ( $f_{\text{HI}}^{\text{CCAE}}$ ) based on the encoded input. Both will use the same encoder, and the input of each head is thus given by  $\mathcal{E}(X)$ .

At the core of the CGGD optimization procedure, the update of the model parameters is defined in Eq. (6). Here  $\theta_j$  is the value of a learnable weight on iteration  $j$  and  $\theta_{j+1}$  the value of the same learnable weight in the next iteration,  $R_{\text{mono}}$ ,  $R_{\text{ene}}$ ,  $R_{\text{upper}}$ , and  $R_{\text{lower}}$  are the rescale factors, which control the relative weight of the different constraints compared to the loss function, for the monotonic degradation constraint, the energy-HI consistency constraint, the upper bound on the HI, and the lower bound on the HI, respectively,  $\eta$  is the learning

rate,  $F_{\text{MH}}$  is a function that balances the gradients of the different heads appropriately,  $\nabla_{\mathcal{E}}$  is the gradient with respect to the latent space determined by the encoder  $\mathcal{E}$ , and  $0 < \epsilon < 1$  to ensure there is a minimum step size in case the gradients from the reconstruction loss to the encodings are very small. A small adaptation to standard CGGD can be observed as the variable  $F_{\text{MH}}$  is included. This is required as  $\theta_{\text{HI}}$  are only trained using the constraints, while  $\theta_{\mathcal{D}}$  are only trained with a loss function. Therefore, the first shared space by both objectives is the encoding space. In this space, the constraints should be prioritized over the reconstruction loss function, as the final model should satisfy the constraints on the training data. The constraints and the loss function will determine an update vector for the encoding space. In order to make sure that the update vector linked to the constraints dominates the model updating both update vectors are set to the same norm. This is accomplished by first setting the update vector created by the constraints to have a unit norm, after which it is multiplied by the norm of the update vector that is calculated based on the loss function. To have a unit norm for the constraints-based update vector, first the gradient of the direction function ( $\text{dir}$ ) is multiplied by the automatic differentiation of the predicted HI ( $f_{\text{HI}}^{\text{CCAE}}(\mathcal{E}(X))$ ) for each encoding space dimension. Then, to let it have unit norm this update vector is multiplied by the rescale factor of the constraint and  $F_{\text{MH}}$  which is defined as:

$$F_{\text{MH}}(X_t, \text{dir}(X_t, \cdot)) := \frac{\|\text{dir}(X_t, \cdot)\|}{\|\nabla_{\mathcal{E}} [\text{dir}(X_t, \cdot) f_{\text{HI}}^{\text{CCAE}}(\mathcal{E}(X_t))]\|}.$$

After being rescaled with  $F_{\text{MH}}$ , the constraint update vector is multiplied by  $\|\nabla_{\mathcal{E}} \mathcal{L}_{\text{reconn}}(X_t, \theta_{\mathcal{E}}, \theta_{\mathcal{D}})\|$ , as can be seen in Eq. (6), to let both the constraint and loss update vector have the same norm.

To train the neural network, an off-the-shelf Adam optimizer is used by applying Eq. (6) iteratively for all learnable parameters. Observe that the partial derivatives of the loss function with respect to  $\theta_{\text{HI}}$  are 0 as they are independent from each other and the partial derivatives of the encodings with respect to  $\theta_{\mathcal{D}}$  are 0 as well as the weights of the decoder are independent from the encodings.

All rescale factors are assumed to be strictly greater than 1, as they represent the relative weight of the constraints compared to the loss function by the definition of CGGD. Different values can be assigned to individual rescale factors to prioritize certain constraints over others. Generally, the constraint with the largest rescale factor takes precedence over all other constraints and the loss function.

In this work, the rescale factor for the monotonic degradation constraint is dynamically adjusted for each individual prediction based on its deviation from the ground truth, within

$$\theta_{j+1} := \theta_j - \eta \left( \frac{\partial \mathcal{L}_{\text{reconn}}(X_t, \boldsymbol{\theta}_{\mathcal{E}}, \boldsymbol{\theta}_{\mathcal{D}})}{\partial \theta_j} + \max \{ \|\nabla_{\mathcal{E}} \mathcal{L}_{\text{reconn}}(X_t, \boldsymbol{\theta}_{\mathcal{E}}, \boldsymbol{\theta}_{\mathcal{D}})\|, \epsilon \} \frac{\partial f_{\text{HI}}^{\text{CCAE}}(\mathcal{E}(X_t))}{\partial \theta_j} \right) \quad (6)$$

$$\left[ R_{\text{mono}} \text{dir}_{\text{mono}}(X_t, \mathbf{X}, \mathbf{t}, \boldsymbol{\theta}_{\mathcal{E}}, \boldsymbol{\theta}_{\text{HI}}) F_{\text{MH}}(X_t, \text{dir}_{\text{mono}}(X_t, \mathbf{X}, \mathbf{t}, \boldsymbol{\theta}_{\mathcal{E}}, \boldsymbol{\theta}_{\text{HI}})) \right. \\ \left. + R_{\text{ene}} \text{dir}_{\text{ene}}(X_t, X_{t_0}, \boldsymbol{\theta}_{\mathcal{E}}, \boldsymbol{\theta}_{\text{HI}}) F_{\text{MH}}(X_t, \text{dir}_{\text{ene}}(X_t, X_{t_0}, \boldsymbol{\theta}_{\mathcal{E}}, \boldsymbol{\theta}_{\text{HI}})) \right. \\ \left. + R_{\text{upper}} \text{dir}_{\text{upper}}(X_t, \boldsymbol{\theta}_{\mathcal{E}}, \boldsymbol{\theta}_{\text{HI}}) F_{\text{MH}}(X_t, \text{dir}_{\text{upper}}(X_t, \boldsymbol{\theta}_{\mathcal{E}}, \boldsymbol{\theta}_{\text{HI}})) \right. \\ \left. + R_{\text{lower}} \text{dir}_{\text{lower}}(X_t, \boldsymbol{\theta}_{\mathcal{E}}, \boldsymbol{\theta}_{\text{HI}}) F_{\text{MH}}(X_t, \text{dir}_{\text{lower}}(X_t, \boldsymbol{\theta}_{\mathcal{E}}, \boldsymbol{\theta}_{\text{HI}})) \right]$$

a bounded interval defined by  $[R_{\text{mono\_lw}}, R_{\text{mono\_up}}]$ . This interval ensures higher rescale factors for larger deviations between the predicted and true ranks and comparatively lower factors for smaller deviations. For a monotonicity direction ( $\text{dir}_{\text{mono}}(X_t, \mathbf{X}, \mathbf{t}, \boldsymbol{\theta}_{\mathcal{E}}, \boldsymbol{\theta}_{\text{HI}})$ ) calculated for sample  $X_t$ , the monotonic rescale factor is calculated as:

$$R_{\text{mono}_t} = R_{\text{mono\_lw}} + \frac{(R_{\text{mono\_up}} - R_{\text{mono\_lw}}) \text{dir}_{\text{mono}}(X_t, \mathbf{X}, \mathbf{t}, \boldsymbol{\theta}_{\mathcal{E}}, \boldsymbol{\theta}_{\text{HI}})}{\text{batch\_size} - 1}$$

Here,  $\text{batch\_size} - 1$  represents an upper bound on the absolute value of the values in  $\text{dir}_{\text{mono}}$ . In particular, this upper bound can be attained when all samples are from the same run and the earliest sample is predicted as the last sample or the other way around.

#### 2.4. Comparison Baselines

To evaluate the effectiveness of the proposed CGGD-based approach, it was compared to two baseline methods. The first baseline is a standard CAE method in which the encoder and decoder parameters are learned according to Eq. (1). Hence, there is no additional head  $f_{\text{HI}}^{\text{CCAE}}$  and there are no added constraints.

The second baseline incorporates the monotonic degradation property using a regularization term in the loss function of the model, unlike the proposed CCAE method, which applies it as a constraint during learning. However, if conventional ranking operations are used for the monotonic degradation loss function, they will create discrete, piecewise-constant outputs, like integer ranks, that are not differentiable. This poses challenges for gradient backpropagation in DL due to null or undefined derivatives. To overcome these issues, the method proposed by Blondel, Teboul, Berthet, and Djolonga (2020) was used.

The method casts the ranking as a projection onto the permutahedron (the convex hull of all permutation vectors). As a result, it creates projection operators that are differentiable, making them suitable for formal analysis. For a given input vector  $(\mathbf{x})$ , the soft rank  $r_{\epsilon}(\mathbf{x})$  is computed as:

$$r_{\epsilon}(\mathbf{x}) = \text{Proj}_{\mathcal{P}}(-\mathbf{x}/\epsilon)$$

where  $\mathcal{P}$  is the permutahedron and  $\epsilon > 0$  is a regularization strength controlling approximation smoothness.

For the predicted HIs ( $f_{\text{HI}}(\mathbf{X})$ ) of set  $\mathbf{X}$ , the soft-rank loss is calculated as:

$$\mathcal{L}_{\text{soft-rank}} = \frac{1}{2} \|r_{\epsilon}(\text{rank}_{\text{asc}}(\mathbf{t})) - r_{\epsilon}(f_{\text{HI}}(\mathbf{X}))\|_2^2, \quad (7)$$

where  $\mathbf{t}$  is a set of timestamps aligned with the samples in set  $\mathbf{X}$ ,  $\text{rank}_{\text{asc}}(\mathbf{t})$  outputs the rank of  $\mathbf{t}$  sorted in ascending order which represents the true ranks and  $r_{\epsilon}(\cdot)$  provides the soft-ranks for the input vectors.

Then, the total loss function of the model is calculated as:

$$\mathcal{L}_{\text{total}} = \mathcal{L}_{\text{reconn}} + \lambda \mathcal{L}_{\text{soft-rank}}, \quad (8)$$

where  $\lambda$  is a trade-off hyperparameter that balances the reconstruction and the soft-rank term.

This second baseline, which incorporates monotonicity as a regularization term in the loss function using the soft-rank approach, is called the soft-rank loss function based CAE (SR-CAE) method.

### 3. EXPERIMENTAL SETUP: BEARING HI ESTIMATION

This section discusses the dataset, the preprocessing and partitioning approach, the model architecture, the setting of the hyperparameters and the relevant evaluation metrics used in this work.

#### 3.1. HI Construction Procedure

The framework for building a predictive model involves several steps, starting with collecting data from monitoring signals such as temperature and vibration to reflect the health of the equipment. This data is then pre-processed to enhance its quality for analysis. An appropriate model is then chosen based on the characteristics of the data and the prognostic needs, with a specific architecture designed to detect bearing degradation patterns. Finally, the model estimates the HIs of bearing health, providing insight into degradation over time.

### 3.2. Pronostia Bearing Degradation Dataset

This work uses the IEEE PHM 2012 Prognostic Challenge dataset, sourced from the Pronostia platform (Patrick Nectoux, Ramasso, & Brigitte Chebel-Morello, 2012). The bearings on this platform are tested under various loads and rotational speeds, comprising 17 run-to-failure datasets of rolling element bearings.

Table 1 summarizes the different conditions and the number of datasets available for training and testing purposes. To perform accelerated degradation tests within a few hours, a high-level radial force was applied that exceeded the maximum dynamic load of the bearings. During these tests, the rotating speed of each bearing was maintained at a stable level. Two accelerometers and a thermocouple were employed to capture vibration signals and bearing temperatures. Vibration signals were recorded using two accelerometers positioned along the vertical and horizontal axes, with a sampling frequency of 25.6kHz and 2560 samples (that is, 1/10 s) collected every 10 seconds.

Since the bearings were subjected to natural degradation, we expect that the degradation patterns will vary between samples. Furthermore, little is known about the specific nature and origin of degradation (for example, whether it involves balls, inner or outer races, or cages), necessitating the application of data-driven techniques (Patrick Nectoux et al., 2012). Failures in any component, ball, rings, or cage could occur simultaneously. The useful life of a bearing is considered to end when the amplitude of the vibration signal exceeds  $20g$ . In this work, only accelerometer data from the provided data set were used as input to estimate the HI.

Conditions	Load (N)	Speed (rpm)	Number of Train Bearings	Number of Test Bearings
1	4000	1800	2	5
2	4200	1650	2	5
3	4500	1300	2	1

Table 1. Summary of the Pronostia dataset.

### 3.3. Preprocessing

Various vibration analysis techniques can be applied to preprocess the raw signals from an accelerometer (Vishwakarma, Purohit, Harshlata, & Rajput, 2017). In this work a similar approach to Meire, Brijder, Dekkers, and Karsmakers (2022) was used, where rich features were calculated that do not include prior knowledge about the bearings. Here, first the acceleration signals are transformed into log-mel spectrograms before using them as input to the machine learning model. The pronostia platform captured recordings of 0.1 seconds or 2560 samples every 10 seconds. To extract the mel spectro-

grams, we processed the vertical and horizontal accelerometer axes using a window size of 0.1 seconds and a hop size of 0.1 seconds. We extract 128 mel bands from each axis, apply logarithmic scaling, and then stack the resulting spectrograms. This creates a 2D input frame with dimensions (128, 2) for each 0.1-second window.

Figure 1 shows a sample of the extracted mel spectrograms from the first bearing that operates under condition 3. At the start of each bearing run, there is a transient behavior likely caused by the initial start-up of the setup. To eliminate this effect, we visually inspect and remove a small section of samples at the beginning of each bearing operation, as demonstrated in Figure 1.

Finally, we normalize the data from each operating condition to achieve zero mean and unit variance across the mel frequency bands, treating each individual axis separately. This normalization is based on the mean and standard deviation calculated from the training set. This normalization helps ensure consistency between different runs under the same conditions.

By transforming raw vibration signals into log-mel spectrograms and applying the appropriate preprocessing steps, we obtain a consistent set of input features to train machine learning models for bearing HI estimation.

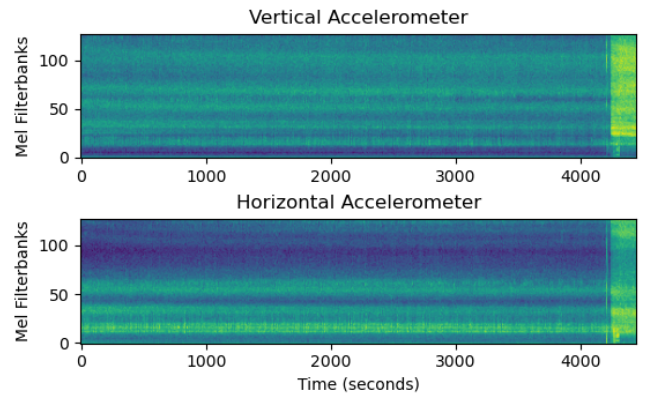


Figure 1. The two axes mel spectral features of a bearing.

### 3.4. Model Architecture

The standard CAE architecture used in this study, illustrated in Figure 2, consists of an encoder with four convolutional layers containing 64, 32, 32, and 16 filters, respectively, followed by a fully connected layer with 16 neurons. The decoder consists of a fully connected layer and 4 deconvolutional layers with 16, 32, 32, and 64 filters, ending with a final deconvolutional layer with two filters, corresponding to the two-axis accelerometer data as the output layer. A batch normalization layer follows each convolutional layer, except the final one. All convolutional layers employ ReLU activation functions and the dense layers use linear activation func-

tions. The convolutional filters used are 1D with a kernel size of 3 and move with a stride of 2. In CCAE a second head is added on top of the encoder output (upper head in Figure 2) to estimate the HI. This second head is composed of three fully connected layers that have 16, 8, and 4 neurons, and the final layer providing a single HI estimate. The hyperparameters used in this model include the Adam optimizer with a learning rate of  $1 \times 10^{-3}$ , an early stopping criterion with a patience of 10 epochs, a batch size of 64. To ensure a standardized comparison of the methodologies, neither regularization nor dropout techniques are implemented in the architecture used.

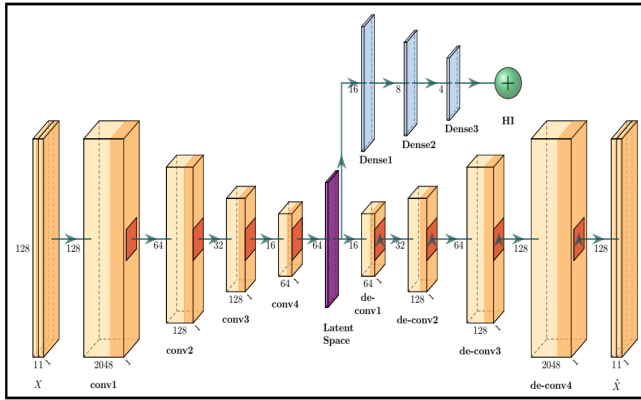


Figure 2. The CCAE Model Architecture.

The final architecture and hyperparameters are selected after conducting multiple experiments to fine-tune them. This is done through a systematic evaluation of various configurations based on reconstruction error and validation accuracy.

### 3.5. Data Set Partitioning

In this work, two bearing runs are used to train the model, while the remaining runs are reserved for testing under each operational condition, as specified in the original PHM challenge (Patrick Nectoux et al., 2012). The training set for each condition is relatively small due to the limited number of runs available. Furthermore, fault patterns and bearing lifetimes can vary significantly, even under identical conditions, complicating the HI estimation. This variability is illustrated in Figure 3, which shows the degradation processes of seven bearings that operate under a similar condition. Although the energy of these bearings is expected to follow a generally increasing trend, the progression towards failure varies considerably among them. Notably, certain bearings, such as B2 and B3, exhibit large energy fluctuations rather than a smooth transition.

From the log-mel spectral features, input batches are created in a structured manner. First, we determine how many samples from each run will comprise a batch, ensuring that each run contributes proportionally to the overall batch size. To

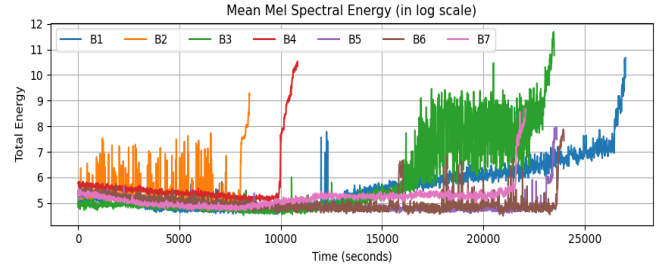


Figure 3. Mean Mel Energy Progression Over Time for Bearings in Operational Condition 1.

enhance representativeness, each run is divided into three sections.

1. **Healthy State:** The first section comprises the initial 10% of the run, assumed to reflect a fully healthy state.
2. **Slight Degradation Phase:** The second section includes samples from 10% to 95% of the run, representing a phase of slight degradation.
3. **Sharp Degradation Phase:** The final section, expected to roughly begin after 95% of the samples in a run, characterizes rapid degradation leading up to apparent failure.

The batches are then created by randomly sampling from each section of the training runs used. Each batch is composed of 20%, 70%, and 10% samples from the healthy state, the slight degradation phase, and the sharp degradation phase, respectively. This method ensures that batches include a balanced representation of data from all phases of degradation, enhancing the training process. To evaluate the performance of each HI estimation method, each experiment was repeated 10 times using different random seeds for batch generation and model initialization. For each scenario, data from the two selected training bearings were combined and shuffled. Of this combined dataset, 75% is used for training, while the remaining 25% is set aside for validation.

### 3.6. HI Evaluation Metrics

The effectiveness of the constructed HI estimates are assessed using three key metrics: trendability, robustness, and consistency (Lei et al., 2018).

#### 3.6.1. Trendability

As operating time increases, components are expected to gradually degrade. Consequently, the degradation trend of an HI should correlate with the operating time. The trendability metric is used as a quantitative measure to evaluate how well HI reflects changes in the condition of a machine over time. To evaluate this correlation in nonlinear degradation trends, we use the Spearman coefficient as the trendability metric, defined as follows (Carino, Zurita, Delgado, Ortega,

& Romero-Troncoso, 2015):

$$\text{Tre}(f_{\text{HI}}(\mathbf{X}), \mathbf{t}) = 1 - \frac{6 \sum_{i=1}^N (\text{rank}(f_{\text{HI}}(X_i)) - \text{rank}(t_i))^2}{N(N^2 - 1)}, \quad (9)$$

where  $N$  is the number of samples,  $\text{rank}(f_{\text{HI}}(X_i))$  and  $\text{rank}(t_i)$  are the ranks of the estimated HI values and the corresponding time value, respectively. The value of  $\text{Tre}(f_{\text{HI}}(\mathbf{X}), \mathbf{t})$  ranges from -1 to 1, approaching either end when there is a strong positive or negative correlation between HI and time.  $\text{Tre}(f_{\text{HI}}(\mathbf{X}), \mathbf{t}) = 1$  means the health indicator is perfectly increasing with time (positive trend).  $\text{Tre}(f_{\text{HI}}(\mathbf{X}), \mathbf{t}) = -1$  means the health indicator is perfectly decreasing with time (negative trend) and  $\text{Tre}(f_{\text{HI}}(\mathbf{X}), \mathbf{t}) = 0$  indicates that there is no trend. The aim of the constraint is to achieve a value of -1.

### 3.6.2. Robustness

A suitable HI should also be robust against inherent interference while maintaining a smooth degradation trend. This property is quantified by the robustness metric (Zhang, Zhang, & Xu, 2016), defined as:

$$\text{Rob}(f_{\text{HI}}(\mathbf{X}), \mathbf{t}) = \frac{1}{N} \sum_{i=1}^N \exp \left( - \left| \frac{f_{\text{HI}}(X_i) - f_{\text{HI}}^s(t_i, \mathbf{X}, \mathbf{t})}{f_{\text{HI}}(X_i)} \right| \right), \quad (10)$$

where  $f_{\text{HI}}^s(t_i, \mathbf{X}, \mathbf{t})$  is a smoothed HI value at  $t_i$ . The smoothing is performed in this work using locally weighted regression (LOESS) (Cleveland & Devlin, 1988; Duong et al., 2018) where each smoothed value is determined using neighboring data points within a specified range.

### 3.6.3. Consistency

Consistency refers to the degree of correlation among multiple HIs. When examining different HI estimates from a single unit, it is expected that they will exhibit some level of correlation because they all reflect the same degradation process. This metric is especially useful in situations where multiple predictions are made, as it enables the assessment of the consistency between these predictions.

Mosallam, Medjaher, and Zerhouni (2016) proposed a consistency metric based on the pairwise symmetrical uncertainty, defined as:

$$\text{Con}(f_{\text{HI}}(\mathbf{X}_1), f_{\text{HI}}(\mathbf{X}_2)) = \frac{2I(f_{\text{HI}}(\mathbf{X}_1), f_{\text{HI}}(\mathbf{X}_2))}{H(f_{\text{HI}}(\mathbf{X}_1)) + H(f_{\text{HI}}(\mathbf{X}_2))}, \quad (11)$$

Where,  $I(f_{\text{HI}}(\mathbf{X}_1), f_{\text{HI}}(\mathbf{X}_2))$  represents the mutual information and  $H(f_{\text{HI}}(\mathbf{X}_1))$  and  $H(f_{\text{HI}}(\mathbf{X}_2))$  denote the entropies of  $f_{\text{HI}}(\mathbf{X}_1)$  and  $f_{\text{HI}}(\mathbf{X}_2)$ , respectively. The output value,  $\text{Con}(f_{\text{HI}}(\mathbf{X}_1), f_{\text{HI}}(\mathbf{X}_2))$ , is normalized to a range between 0 and 1. A higher value indicates a greater similarity between

the two HIs, suggesting a stronger consistency. For multiple HI estimates, pairwise consistency values are computed and the final consistency metric is determined by taking the mean and standard deviation of these pairwise results.

## 4. EVALUATION OF HI ESTIMATION METHODS: EXPERIMENTAL RESULTS AND DISCUSSION

This section presents the experimental results, starting with a comparative analysis of the proposed CCAE method against two baselines: the standard CAE and the SR-CAE methods. This is followed by a detailed discussion of all methods based on the performance metrics described in Section 3.6. When comparing results, if the models show the same mean performance metric, the one with a smaller standard deviation is considered better. For each bearing under the three operating conditions, the first two bearing data are used for training, while the remaining bearing data are set aside for testing.

### 4.1. General Comparative Analysis

The overall performance of each approach is visually assessed by analyzing the results of the bearings in Condition 3 across the three HI estimation methods. This analysis provides a general overview, providing insight into how effectively each technique estimates the health degradation of bearings. In all HI estimation plots presented in this work, the smoothing (red line) is done using LOESS.

Figure 4 illustrates the degradation patterns using the standard CAE HI estimation method. Here, HI estimates might not decrease consistently, even in the training data, highlighting challenges related to the generalizability of this approach. Furthermore, the reconstruction error varies considerably across different bearings, despite operating under similar conditions. This results in varying HI values, making it difficult to establish a reliable correlation between these values and the actual state of bearing health.

Figure 5 presents the HI estimates using the SR-CAE method. This is an alternative approach to enforce monotonicity by regularizing the loss function. In this method, the influences of both the reconstruction and the soft-rank losses on the gradients of the CAE architecture are equally weighted, with the hyperparameter  $\lambda$  set to 1 in Eq. (8). Although this method demonstrates much improved monotonic degradation behavior, there remains considerable variation in HI values between different bearings. Notably, even in the training sets, substantial differences are observed at both the beginning of the operation and near the failure points.

In the CCAE method, different rescale factors are applied to the constraints: [1.25, 1.5] for the monotonicity constraint, 1.5 for the energy-HI consistency constraint and 2.0 for both the upper and lower HI boundary constraints. Prioritizing boundary constraints ensures that the predicted HI values re-

main within the interval  $[0, 1]$ . Lowering the priority on boundary constraints increases the chances that the predictions fall outside of this range. The HI estimates based on CCAE provide several advantages over the baseline methods, as shown in Figure 6. It produces a smoother degradation profile, indicating a more consistent decline in bearing health over time. The HI values range from 1 (indicating a fully healthy state) to 0 (indicating complete failure), which aligns well with the expected physical degradation process. In addition, the degradation curves correspond to typical bearing degradation, exhibiting a steady decline during the initial phase followed by rapid deterioration as the bearing approaches failure. As a result, the CCAE approach provides a more accurate and reliable representation of bearing health compared to the baseline methods.

#### 4.2. Comparison of Standard CAE and CCAE Methods

The standard CAE model is trained using the initial 10% of the training bearing data, which roughly represents the healthy phase of the bearing operation. During this phase, the model reconstruction error is close to zero. However, as the bearing operation time increases, the reconstruction error increases, indicating a degradation in bearing health and a progression towards failure.

Table 2 summarizes the performance metrics of the standard CAE method compared to that of the CCAE method for all the training and test bearings. The results show that CCAE outperforms the standard CAE in trendability and consistency by more than 75% and robustness close to 65% considering all the bearings. These results demonstrate that the CCAE method more effectively tracks the degradation of the bearings over time. It also provides robust, consistent, and repeatable HI estimates across multiple runs. In some cases, while the standard CAE method might yield superior results, these observations may not fully capture the overall performance of the method. Specifically, for Bearing\_2\_3, the trendability metric value for the standard CAE method is  $-0.732$ , which is significantly lower than the  $-0.092$  obtained for CCAE. Although this value suggests a better decreasing correlation of HI with time, the HI value actually increases as the bearing approaches failure, contradicting the expected full-run decreasing trend, as depicted in Figure 7. In contrast, the CCAE method, despite having a lower trendability metric, accurately reflects the expected decrease in HI values as the bearing approaches failure, as shown in Figure 8. In addition, for Bearing\_2\_3 the HI value for the healthiest condition is close to  $-50$ , approximately 2500 seconds into its operation, and at the end. In contrast, Bearing\_2\_5 approaches an HI value of  $-50$  near failure. This inconsistency, where one bearing's healthiest HI value is close to another bearing's failure point, underscores the challenge of obtaining a generally representative HI estimates using the standard CAE method.

Further insights into performance discrepancies are provided by examining bearings from condition 1 in figures 9 and 10. Figure 3 shows that Bearing\_1\_3 experiences significant energy fluctuations after 16,000 seconds. These fluctuations are reflected in the HI estimates of both methods. However, in the case of standard CAE, the HI values increase as the failure approach, contrary to expectations of a decreasing trend. However, CCAE minimizes these fluctuations and maintains HI values that align with the expected degradation trajectory. For Bearing\_1\_7, the trendability metric for the standard CAE HI estimation approach achieves  $-0.610$ , outperforming the CCAE score of 0.339. Despite this higher trendability score for CCAE, a notable advantage is that its HI values are bounded within a range of 0 to 1, providing a more interpretable measure of health status.

In general, the CCAE method improves on the standard CAE HI estimation approach by providing more consistent HI estimates. It is generalizable and robust, handling noisy and unseen test data much better.

#### 4.3. Comparison of Soft-Rank Loss Function based CAE and CCAE Methods

Table 3 provides a detailed comparison of the performance of the SR-CAE HI estimation method compared to the CCAE method across all bearings. The results indicate that the SR-CAE method surpasses the CCAE method in trendability for more than 95% bearings. In contrast, the CCAE method outperforms the SR-CAE method in robustness for more than 95% of the bearings and exhibits greater consistency for nearly 90% of the bearings with smaller overall variance.

The advantage of the SR-CAE method in trendability comes from its objective function, which minimizes the reconstruction loss while enforcing a decreasing monotonicity in the HI estimates without constraints, resulting in a more monotonic degradation pattern. However, CCAE demonstrates superior robustness and consistency, showing less variability in HI estimates. This suggests more stable degradation trends and smoother transitions in HI values over time. Furthermore, for multiple HI estimates, the results consistently provide stable and replicable values.

Figure 11 provides a validation of these results. The improved monotonicity of the HI values is notably apparent in Bearing\_2\_3 when using the SR-CAE method, as opposed to CCAE. However, significant variability in HI values is observed in both Bearing\_2\_3 and Bearing\_2\_5 along their lifetime with the SR-CAE method, unlike CCAE shown in Figure 8. Such disparities complicate the generalizability of the SR-CAE method when compared to the CCAE method.

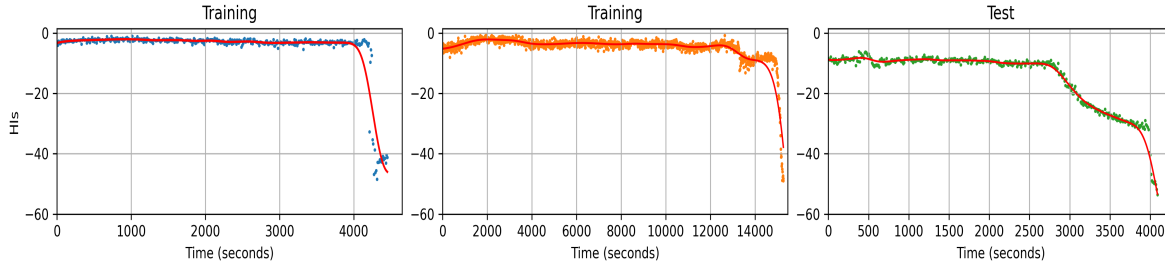


Figure 4. Standard CAE based HI estimates for condition 3 Bearing\_3\_1, Bearing\_3\_2 and Bearing\_3\_3.

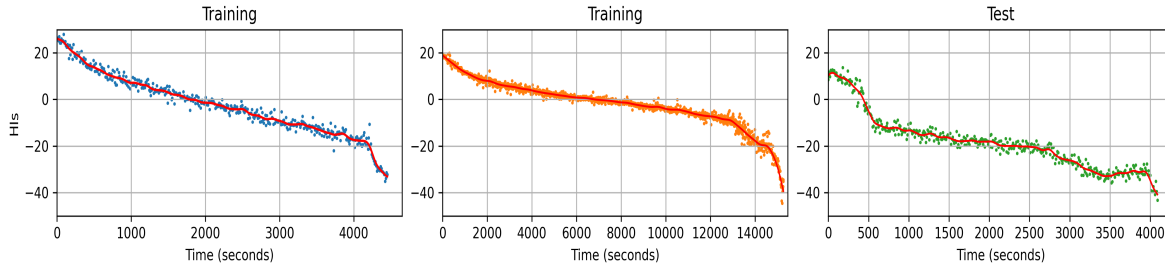


Figure 5. SR-CAE based HI estimates for condition 3 Bearing\_3\_1, Bearing\_3\_2 and Bearing\_3\_3.

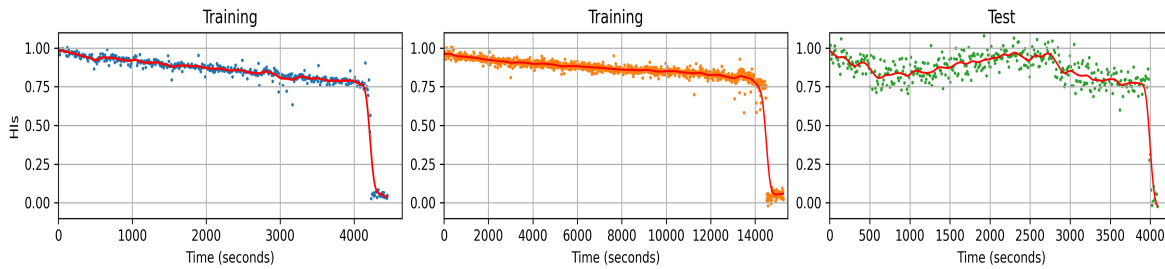


Figure 6. CCAE based HI estimates for condition 3 Bearing\_3\_1, Bearing\_3\_2 and Bearing\_3\_3.

Bearings	Standard CAE based HI Estimation			CCAE based HI Estimation		
	Trendability	Robustness	Consistency	Trendability	Robustness	Consistency
Bearing_1_1	$-0.180 \pm 0.026$	<b><math>0.954 \pm 0.001</math></b>	<b><math>0.985 \pm 0.012</math></b>	$-0.991 \pm 0.005$	$0.946 \pm 0.003$	$0.921 \pm 0.070$
Bearing_1_2	$-0.464 \pm 0.055$	$0.940 \pm 0.003$	<b><math>0.877 \pm 0.101</math></b>	$-0.963 \pm 0.019$	<b><math>0.941 \pm 0.005</math></b>	$0.723 \pm 0.244$
Bearing_1_3	$0.324 \pm 0.027$	$0.936 \pm 0.003$	$0.691 \pm 0.199$	$-0.392 \pm 0.394$	<b><math>0.946 \pm 0.016</math></b>	<b><math>0.856 \pm 0.091</math></b>
Bearing_1_4	$-0.772 \pm 0.020$	$0.942 \pm 0.001$	<b><math>0.929 \pm 0.056</math></b>	$-0.785 \pm 0.109$	<b><math>0.948 \pm 0.016</math></b>	$0.814 \pm 0.147$
Bearing_1_5	$0.597 \pm 0.077$	<b><math>0.972 \pm 0.002</math></b>	$0.772 \pm 0.171$	<b><math>0.316 \pm 0.247</math></b>	$0.946 \pm 0.006$	<b><math>0.922 \pm 0.073</math></b>
Bearing_1_6	$0.446 \pm 0.117$	$0.916 \pm 0.004$	$0.883 \pm 0.089$	<b><math>0.157 \pm 0.227</math></b>	<b><math>0.922 \pm 0.009</math></b>	<b><math>0.938 \pm 0.059</math></b>
Bearing_1_7	<b><math>-0.629 \pm 0.121</math></b>	<b><math>0.966 \pm 0.002</math></b>	$0.899 \pm 0.083$	$0.339 \pm 0.248$	$0.948 \pm 0.004$	<b><math>0.949 \pm 0.046</math></b>
Bearing_2_1	$-0.568 \pm 0.004$	$0.927 \pm 0.001$	$0.915 \pm 0.025$	<b><math>-0.983 \pm 0.000</math></b>	<b><math>0.943 \pm 0.004</math></b>	<b><math>0.922 \pm 0.070</math></b>
Bearing_2_2	$0.397 \pm 0.030$	$0.948 \pm 0.002$	$0.944 \pm 0.025$	<b><math>-0.981 \pm 0.001</math></b>	<b><math>0.949 \pm 0.006</math></b>	<b><math>0.959 \pm 0.040</math></b>
Bearing_2_3	<b><math>-0.732 \pm 0.005</math></b>	<b><math>0.975 \pm 0.008</math></b>	$0.602 \pm 0.224$	$-0.092 \pm 0.337$	$0.879 \pm 0.091$	<b><math>0.743 \pm 0.184</math></b>
Bearing_2_4	$0.381 \pm 0.108$	$0.926 \pm 0.002$	$0.816 \pm 0.208$	<b><math>-0.665 \pm 0.143</math></b>	<b><math>0.930 \pm 0.008</math></b>	<b><math>0.937 \pm 0.066</math></b>
Bearing_2_5	<b><math>-0.856 \pm 0.051</math></b>	<b><math>0.921 \pm 0.002</math></b>	$0.850 \pm 0.142$	$-0.054 \pm 0.488$	$0.874 \pm 0.034$	<b><math>0.896 \pm 0.082</math></b>
Bearing_2_6	$0.683 \pm 0.016$	$0.915 \pm 0.005$	$0.864 \pm 0.117$	<b><math>-0.220 \pm 0.462</math></b>	<b><math>0.917 \pm 0.009</math></b>	<b><math>0.907 \pm 0.083</math></b>
Bearing_2_7	$-0.472 \pm 0.027$	$0.846 \pm 0.009$	$0.507 \pm 0.346$	<b><math>-0.506 \pm 0.320</math></b>	<b><math>0.879 \pm 0.107</math></b>	<b><math>0.600 \pm 0.365</math></b>
Bearing_3_1	$-0.134 \pm 0.088$	$0.930 \pm 0.004$	$0.533 \pm 0.343$	<b><math>-0.947 \pm 0.009</math></b>	<b><math>0.938 \pm 0.005</math></b>	<b><math>0.946 \pm 0.057</math></b>
Bearing_3_2	$-0.565 \pm 0.078$	$0.925 \pm 0.003$	<b><math>0.982 \pm 0.012</math></b>	<b><math>-0.955 \pm 0.008</math></b>	<b><math>0.943 \pm 0.004</math></b>	$0.956 \pm 0.045$
Bearing_3_3	<b><math>-0.737 \pm 0.045</math></b>	<b><math>0.966 \pm 0.001</math></b>	$0.850 \pm 0.102$	$-0.599 \pm 0.127$	$0.918 \pm 0.013$	<b><math>0.852 \pm 0.143</math></b>

Table 2. Standard CAE Vs. CCAE based performance evaluations on all bearings.

Bearings	SR-CAE based HI Estimation			CCAЕ based HI Estimation		
	Trendability	Robustness	Consistency	Trendability	Robustness	Consistency
Bearing_1.1	$-0.998 \pm 0.000$	$0.895 \pm 0.009$	$0.915 \pm 0.047$	$-0.991 \pm 0.005$	<b><math>0.946 \pm 0.003</math></b>	<b><math>0.921 \pm 0.070</math></b>
Bearing_1.2	<b><math>-0.989 \pm 0.001</math></b>	$0.859 \pm 0.021$	<b><math>0.860 \pm 0.076</math></b>	$-0.963 \pm 0.019$	<b><math>0.941 \pm 0.005</math></b>	$0.723 \pm 0.244$
Bearing_1.3	<b><math>-0.418 \pm 0.147</math></b>	$0.906 \pm 0.011$	$0.762 \pm 0.113$	$-0.392 \pm 0.394$	<b><math>0.946 \pm 0.016</math></b>	<b><math>0.856 \pm 0.091</math></b>
Bearing_1.4	<b><math>-0.921 \pm 0.025</math></b>	$0.867 \pm 0.047$	<b><math>0.844 \pm 0.149</math></b>	$-0.785 \pm 0.109$	<b><math>0.948 \pm 0.016</math></b>	$0.814 \pm 0.147$
Bearing_1.5	<b><math>-0.537 \pm 0.174</math></b>	$0.552 \pm 0.099$	$0.913 \pm 0.067$	$0.316 \pm 0.247$	<b><math>0.946 \pm 0.006</math></b>	<b><math>0.922 \pm 0.073</math></b>
Bearing_1.6	<b><math>-0.500 \pm 0.130</math></b>	$0.812 \pm 0.054$	$0.901 \pm 0.114$	$0.157 \pm 0.227$	<b><math>0.922 \pm 0.009</math></b>	<b><math>0.938 \pm 0.059</math></b>
Bearing_1.7	<b><math>-0.868 \pm 0.021</math></b>	$0.636 \pm 0.026$	$0.930 \pm 0.055$	$0.339 \pm 0.248$	<b><math>0.948 \pm 0.004</math></b>	<b><math>0.949 \pm 0.046</math></b>
Bearing_2.1	<b><math>-0.995 \pm 0.001</math></b>	$0.896 \pm 0.008$	$0.825 \pm 0.113$	$-0.983 \pm 0.000$	<b><math>0.943 \pm 0.004</math></b>	<b><math>0.922 \pm 0.070</math></b>
Bearing_2.2	<b><math>-0.997 \pm 0.000</math></b>	$0.893 \pm 0.005$	$0.917 \pm 0.057$	$-0.981 \pm 0.001$	<b><math>0.949 \pm 0.006</math></b>	<b><math>0.959 \pm 0.040</math></b>
Bearing_2.3	<b><math>-0.672 \pm 0.054</math></b>	<b><math>0.938 \pm 0.034</math></b>	$0.666 \pm 0.201$	$-0.092 \pm 0.337$	$0.879 \pm 0.091$	<b><math>0.743 \pm 0.184</math></b>
Bearing_2.4	<b><math>-0.839 \pm 0.040</math></b>	$0.627 \pm 0.048$	$0.789 \pm 0.167$	$-0.665 \pm 0.143$	<b><math>0.930 \pm 0.008</math></b>	<b><math>0.937 \pm 0.066</math></b>
Bearing_2.5	$0.009 \pm 0.156$	$0.710 \pm 0.086$	$0.878 \pm 0.128$	<b><math>-0.054 \pm 0.488</math></b>	<b><math>0.874 \pm 0.037</math></b>	<b><math>0.896 \pm 0.082</math></b>
Bearing_2.6	<b><math>-0.500 \pm 0.201</math></b>	$0.774 \pm 0.046$	$0.829 \pm 0.161$	$-0.220 \pm 0.462$	<b><math>0.917 \pm 0.009</math></b>	<b><math>0.907 \pm 0.083</math></b>
Bearing_2.7	<b><math>-0.803 \pm 0.071</math></b>	$0.845 \pm 0.112$	$0.423 \pm 0.332$	$-0.506 \pm 0.320$	<b><math>0.879 \pm 0.107</math></b>	<b><math>0.600 \pm 0.365</math></b>
Bearing_3.1	<b><math>-0.988 \pm 0.002</math></b>	$0.805 \pm 0.004$	$0.927 \pm 0.032$	$-0.947 \pm 0.009$	<b><math>0.938 \pm 0.005</math></b>	<b><math>0.946 \pm 0.057</math></b>
Bearing_3.2	<b><math>-0.995 \pm 0.001</math></b>	$0.838 \pm 0.012$	$0.932 \pm 0.056$	$-0.955 \pm 0.008$	<b><math>0.943 \pm 0.004</math></b>	<b><math>0.956 \pm 0.045</math></b>
Bearing_3.3	<b><math>-0.966 \pm 0.005</math></b>	$0.884 \pm 0.017$	$0.805 \pm 0.135$	$-0.599 \pm 0.127$	<b><math>0.918 \pm 0.013</math></b>	<b><math>0.852 \pm 0.143</math></b>

Table 3. SR-CAE Vs. CCAE performance evaluations on all bearings.

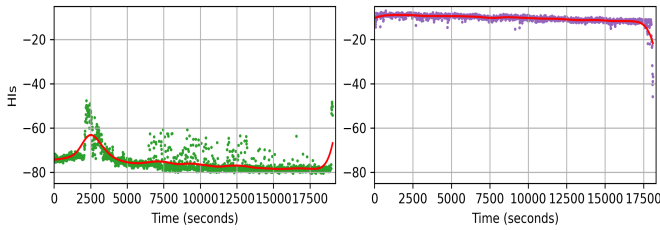


Figure 7. Standard CAE based HI estimates for Bearing\_2\_3 and Bearing\_2\_5.

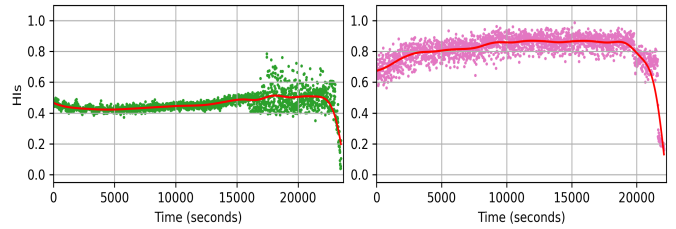


Figure 10. CCAE based HI estimates for Bearing\_1\_3 and Bearing\_1\_7.

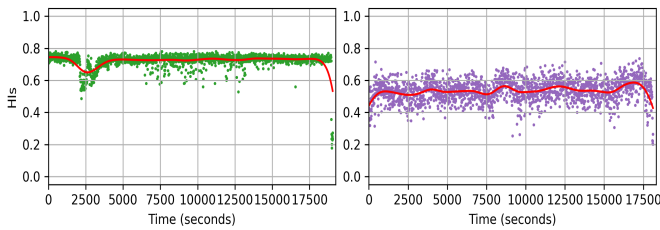


Figure 8. CCAE based HI estimates for Bearing\_2\_3 and Bearing\_2\_5.

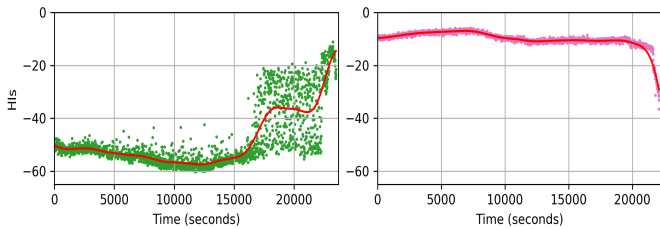


Figure 9. Standard CAE based HI estimates for Bearing\_1\_3 and Bearing\_1\_7.

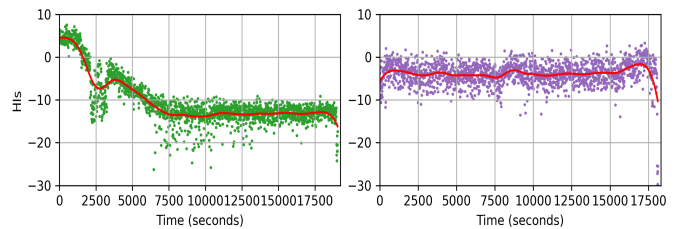


Figure 11. SR-CAE based HI estimates for Bearing\_2\_3 and Bearing\_2\_5.

## 5. ABLATION STUDY

In this section, we analyze the effects of modifying various aspects of the complete implementation of the CCAE method. Specifically, we examine the impact of individual constraints within the CCAE method, the influence of different constraint rescale factors, and the effect of replacing the monotonicity constraint with a soft-rank loss function in the CCAE method.

### 5.1. Impact of Constraints on CCAE

In this section, we examine the impact of each constraint in the CCAE implementation by systematically excluding one constraint at a time and evaluating the resulting performance. The experiments devised for this study are the following:

1. **CCAEBB**: The monotonicity constraint is excluded. However, the energy-HI consistency and boundary constraints are retained, with rescale factors of 1.5 and 2.0, respectively.
2. **CCAEMB**: The energy-HI consistency constraint is excluded. However, monotonicity and boundary constraints are retained, with rescale factors of [1.25, 1.5] and 2.0, respectively.
3. **CCAEME**: The boundary constraints are excluded, leaving only the monotonicity and energy-HI consistency constraints, with rescale factors of [1.25, 1.5] and 1.5, respectively.

The results of this experiment, presented in Table 4, highlight the importance of the different constraints in the CCAE method. The monotonicity constraint significantly enhances the trendability of the HI estimates, as its primary objective is to enforce the progressive health degradation of the bearings. The boundary constraint plays a crucial role in maintaining the consistency of the HI estimates by ensuring that they remain within the defined range of [0, 1], leading to reliable HI estimates across multiple experiments. Furthermore, the energy-HI consistency constraint contributes to both robustness and consistency. Its formulation penalizes high fluctuations in HI predictions that do not align with the energy progression of the signal, thereby providing a smooth and reliable degradation trend over time. Ultimately, all constraints play a vital role in enforcing the desired properties expected of the bearing HI estimates. By incorporating all these constraints, the CCAE approach effectively captures the degradation pattern while ensuring robustness and consistency in the HI estimates.

### 5.2. Effects of Rescale Factors on CCAE

This section examines the impact of the selection of the rescale factors on the performance of CCAE. The objective of this experiment is to assess the stability of the CCAE method, demonstrating that small changes to the rescale factors do not lead to significant performance fluctuations. Building on

the results from Section 4.2, where the rescale factors [1.25, 1.5], 1.5, 2.0, and 2.0 (referred as RF\_C1) were applied to the monotonicity, energy-HI consistency, upper and lower boundary constraints, we conduct additional experiment to evaluate the effect of small variations in these factors. To this end, we examine an alternative set of rescale factors: [1.05, 1.25], 1.25, 1.25, and 1.25 (referred as RF\_C2).

The results of this experiment, presented in Table 5, highlight the performance differences of the CCAE method when using different constraint rescale factors. The findings indicate that in terms of trendability, RF\_C2 slightly outperforms RF\_C1 in 58.82% of the bearings. Both models show minimal variability, with the largest observed differences being  $-0.322 \pm 0.228$  for RF\_C1 and  $-0.092 \pm 0.337$  for RF\_C2 in Bearing\_2\_3. When comparing robustness, RF\_C1 outperforms RF\_C2 in 58.82% of the bearings. This suggests a slight overall advantage for RF\_C1. Furthermore, the variability between the models for robustness remains minimal, with the largest differences being  $0.922 \pm 0.018$  for RF\_C1 and  $0.879 \pm 0.107$  for RF\_C2 in Bearing\_2\_7. In terms of consistency, RF\_C2 demonstrates superior performance over RF\_C1 in 64.71% of the bearings. This improvement is attributed to the larger boundary constraint rescale factor used in RF\_C2. The largest differences in consistency are observed in Bearing\_1\_6, where RF\_C1 achieves  $0.839 \pm 0.119$  and RF\_C2 has a value of  $0.938 \pm 0.059$ .

Overall, the results indicate that the performance of both approaches is comparable, and small changes in rescale factors do not lead to significant performance fluctuations.

### 5.3. Soft Rank based CCAE

In this approach, the modification of CCAE involves replacing the monotonic degradation constraint with a soft-ranking in the loss function. The influences of the reconstruction and the soft-rank losses on the gradients of the model architecture are equally weighted, with a value of  $\lambda$  set to 1 in Eq. (8). Additionally, only the upper and lower bounds are included as constraints, with a rescale factor set to 2.0 and excluding the energy-HI consistency constraint.

Table 6 summarizes the performance comparison between the soft-rank CCAE method and the CCAE method with all constraints across all bearings. The results show that the soft-rank CCAE method outperforms the CCAE method in 82.36% of the bearings based on the trendability metric. This superior performance is especially clear across all test bearings. Although both methods integrate monotonicity behavior differently, the soft-rank CCAE method benefits from having one fewer constraint to satisfy the energy-HI consistency requirement, giving it a clear advantage in the trendability metric. Furthermore, the CCAE method exhibits a 100% advantage in terms of robustness across all bearings, mainly due to the inclusion of the energy-HI consistency constraint. The

Bearings	CCAE_EB			CCAE_MB			CCAE_ME		
	Trendability	Robustness	Consistency	Trendability	Robustness	Consistency	Trendability	Robustness	Consistency
Bearing_1.1	-0.523 ± 0.075	0.923 ± 0.005	<b>0.995 ± 0.004</b>	-0.985 ± 0.003	0.904 ± 0.012	0.958 ± 0.036	<b>-0.994 ± 0.002</b>	<b>0.991 ± 0.001</b>	0.862 ± 0.087
Bearing_1.2	-0.557 ± 0.054	0.930 ± 0.009	0.877 ± 0.147	-0.876 ± 0.027	0.915 ± 0.006	<b>0.935 ± 0.060</b>	<b>-0.966 ± 0.011</b>	<b>0.988 ± 0.002</b>	0.495 ± 0.293
Bearing_1.3	-0.188 ± 0.320	0.875 ± 0.131	0.814 ± 0.112	<b>-0.775 ± 0.205</b>	0.923 ± 0.020	<b>0.911 ± 0.052</b>	-0.064 ± 0.300	<b>0.956 ± 0.011</b>	0.909 ± 0.069
Bearing_1.4	-0.704 ± 0.133	0.909 ± 0.027	0.855 ± 0.107	<b>-0.710 ± 0.224</b>	0.950 ± 0.010	<b>0.895 ± 0.072</b>	-0.629 ± 0.177	<b>0.972 ± 0.005</b>	0.862 ± 0.090
Bearing_1.5	0.230 ± 0.240	0.918 ± 0.020	0.864 ± 0.187	<b>-0.237 ± 0.228</b>	0.934 ± 0.011	<b>0.864 ± 0.142</b>	-0.046 ± 0.296	<b>0.974 ± 0.005</b>	0.838 ± 0.140
Bearing_1.6	0.034 ± 0.153	0.892 ± 0.017	<b>0.927 ± 0.082</b>	<b>-0.433 ± 0.142</b>	0.896 ± 0.031	0.860 ± 0.167	0.028 ± 0.123	<b>0.968 ± 0.007</b>	0.833 ± 0.181
Bearing_1.7	0.407 ± 0.172	0.923 ± 0.010	<b>0.939 ± 0.062</b>	<b>-0.658 ± 0.204</b>	0.935 ± 0.011	0.907 ± 0.075	-0.143 ± 0.388	<b>0.973 ± 0.004</b>	0.929 ± 0.055
Bearing_2.1	-0.622 ± 0.060	0.897 ± 0.006	<b>0.993 ± 0.005</b>	<b>-0.991 ± 0.002</b>	0.937 ± 0.005	0.868 ± 0.128	-0.983 ± 0.003	<b>0.975 ± 0.004</b>	0.671 ± 0.224
Bearing_2.2	-0.598 ± 0.045	0.900 ± 0.006	<b>0.992 ± 0.005</b>	<b>-0.995 ± 0.001</b>	0.944 ± 0.009	0.901 ± 0.093	-0.987 ± 0.005	<b>0.977 ± 0.006</b>	0.863 ± 0.123
Bearing_2.3	-0.264 ± 0.308	0.817 ± 0.169	<b>0.747 ± 0.168</b>	<b>-0.402 ± 0.192</b>	<b>0.858 ± 0.097</b>	0.652 ± 0.197	-0.323 ± 0.201	0.853 ± 0.100	0.682 ± 0.191
Bearing_2.4	-0.638 ± 0.377	0.905 ± 0.027	<b>0.893 ± 0.076</b>	-0.715 ± 0.186	0.925 ± 0.011	0.746 ± 0.254	<b>-0.765 ± 0.120</b>	<b>0.942 ± 0.012</b>	0.732 ± 0.230
Bearing_2.5	0.166 ± 0.306	0.808 ± 0.080	<b>0.918 ± 0.084</b>	<b>-0.180 ± 0.283</b>	0.869 ± 0.044	0.864 ± 0.127	-0.130 ± 0.318	<b>0.916 ± 0.045</b>	0.856 ± 0.139
Bearing_2.6	-0.168 ± 0.322	0.883 ± 0.025	0.899 ± 0.104	-0.387 ± 0.287	0.905 ± 0.014	0.847 ± 0.139	<b>-0.571 ± 0.211</b>	<b>0.937 ± 0.008</b>	<b>0.923 ± 0.081</b>
Bearing_2.7	-0.486 ± 0.234	0.882 ± 0.080	<b>0.563 ± 0.287</b>	<b>-0.611 ± 0.262</b>	0.841 ± 0.127	0.393 ± 0.410	-0.518 ± 0.277	<b>0.892 ± 0.088</b>	0.474 ± 0.353
Bearing_3.1	-0.484 ± 0.038	0.915 ± 0.011	<b>0.969 ± 0.033</b>	<b>-0.981 ± 0.003</b>	0.932 ± 0.006	0.945 ± 0.046	-0.959 ± 0.008	<b>0.983 ± 0.003</b>	0.904 ± 0.104
Bearing_3.2	-0.496 ± 0.027	0.917 ± 0.003	<b>0.992 ± 0.006</b>	<b>-0.991 ± 0.002</b>	0.951 ± 0.006	0.923 ± 0.063	-0.974 ± 0.003	<b>0.986 ± 0.004</b>	0.915 ± 0.062
Bearing_3.3	-0.234 ± 0.317	0.910 ± 0.016	0.898 ± 0.101	<b>-0.769 ± 0.151</b>	0.855 ± 0.030	<b>0.949 ± 0.040</b>	-0.673 ± 0.231	<b>0.954 ± 0.012</b>	0.928 ± 0.069

Table 4. Impact of constraints on CCAE performance on all bearings.

Bearings	RF_C1			RF_C2		
	Trendability	Robustness	Consistency	Trendability	Robustness	Consistency
Bearing_1.1	<b>-0.993 ± 0.002</b>	0.944 ± 0.004	0.908 ± 0.071	-0.991 ± 0.005	<b>0.946 ± 0.003</b>	<b>0.921 ± 0.070</b>
Bearing_1.2	<b>-0.971 ± 0.008</b>	0.940 ± 0.004	<b>0.804 ± 0.111</b>	-0.963 ± 0.019	<b>0.941 ± 0.005</b>	0.723 ± 0.244
Bearing_1.3	-0.313 ± 0.408	<b>0.954 ± 0.006</b>	<b>0.864 ± 0.118</b>	<b>-0.392 ± 0.394</b>	0.946 ± 0.016	0.856 ± 0.091
Bearing_1.4	-0.741 ± 0.188	<b>0.952 ± 0.007</b>	<b>0.878 ± 0.093</b>	<b>-0.785 ± 0.109</b>	0.948 ± 0.016	0.814 ± 0.147
Bearing_1.5	0.331 ± 0.146	<b>0.948 ± 0.006</b>	<b>0.946 ± 0.056</b>	<b>0.316 ± 0.247</b>	0.946 ± 0.006	0.922 ± 0.073
Bearing_1.6	<b>0.108 ± 0.146</b>	<b>0.925 ± 0.017</b>	0.839 ± 0.119	0.157 ± 0.227	0.922 ± 0.009	<b>0.938 ± 0.059</b>
Bearing_1.7	0.359 ± 0.148	<b>0.950 ± 0.005</b>	0.920 ± 0.073	<b>0.339 ± 0.248</b>	0.948 ± 0.004	<b>0.949 ± 0.046</b>
Bearing_2.1	<b>-0.984 ± 0.002</b>	0.939 ± 0.005	<b>0.936 ± 0.078</b>	-0.983 ± 0.000	<b>0.943 ± 0.004</b>	0.922 ± 0.070
Bearing_2.2	-0.981 ± 0.005	0.942 ± 0.003	0.950 ± 0.038	<b>-0.981 ± 0.001</b>	<b>0.949 ± 0.006</b>	<b>0.959 ± 0.040</b>
Bearing_2.3	<b>-0.322 ± 0.228</b>	<b>0.917 ± 0.017</b>	0.737 ± 0.177	-0.092 ± 0.337	0.879 ± 0.091	<b>0.743 ± 0.184</b>
Bearing_2.4	-0.640 ± 0.211	0.924 ± 0.009	0.850 ± 0.168	<b>-0.665 ± 0.143</b>	<b>0.930 ± 0.008</b>	<b>0.937 ± 0.066</b>
Bearing_2.5	<b>-0.165 ± 0.351</b>	0.871 ± 0.030	0.886 ± 0.100	-0.054 ± 0.488	<b>0.874 ± 0.037</b>	<b>0.896 ± 0.082</b>
Bearing_2.6	-0.035 ± 0.291	<b>0.919 ± 0.006</b>	0.879 ± 0.147	<b>-0.220 ± 0.462</b>	0.917 ± 0.009	<b>0.907 ± 0.083</b>
Bearing_2.7	-0.474 ± 0.267	<b>0.922 ± 0.018</b>	0.553 ± 0.324	<b>-0.506 ± 0.320</b>	0.879 ± 0.107	<b>0.600 ± 0.365</b>
Bearing_3.1	<b>-0.948 ± 0.010</b>	<b>0.941 ± 0.009</b>	0.936 ± 0.063	-0.947 ± 0.009	0.938 ± 0.005	<b>0.946 ± 0.057</b>
Bearing_3.2	-0.948 ± 0.013	0.942 ± 0.005	0.938 ± 0.051	<b>-0.955 ± 0.008</b>	<b>0.943 ± 0.004</b>	<b>0.956 ± 0.045</b>
Bearing_3.3	-0.554 ± 0.229	<b>0.922 ± 0.009</b>	<b>0.925 ± 0.063</b>	<b>-0.599 ± 0.127</b>	0.918 ± 0.013	0.852 ± 0.143

Table 5. Effects of rescale factors on CCAE performance on all bearings.

CCAIE method exhibits a higher level of consistency than the soft-rank CCAIE method, showing a 64.71% improvement across all bearings and performing particularly well on the test bearings. In summary, explicitly adding desired properties as constraints during training is advantageous for enhancing model performance. Although adding a particular constraint may decrease a single metric, it can lead to overall improvement when considering all metrics collectively.

## 6. CONCLUSION

In conclusion, this study successfully demonstrates the potential of a constraint-guided deep learning framework, specifically CCAIE, to develop physically consistent health indicators for bearing PHM. By incorporating domain knowledge through monotonicity, boundary and energy-HI consistency constraints, the CCAIE addresses the limitations of both conventional data-driven and physics-based methods. The experimental results show that CCAIE is significantly better than the standard CAE, achieving 65% higher robustness and 75% higher consistency. It also outperforms the SR-CAE baseline with a 95% improvement in robustness and a 90% improvement in consistency. Although the SR-CAE method excels in trendability metrics for 95% of bearings due to the explicit use of monotonicity in model training, CCAIE performs better than CAE for 75% of the bearings. Moreover, the CCAIE generates HI outputs that are bounded within a specified range and reliably represent the bearing's health state. Its degradation profiles are smoother and closely align with expected physical degradation patterns, underscoring the value of incorporating domain knowledge constraints. The ablation study further confirms that the monotonicity constraint enhances trendability, the boundary constraint ensures consistency, and the energy-HI consistency constraint improves robustness. Furthermore, our findings indicate that minor changes in the rescale factor of these constraints do not substantially affect the performance of CCAIE. These findings underscore the potential of employing representative constraints in the proposed deep learning framework to generate reliable bearing HIs. Future research could explore the performance of the framework in other datasets, incorporate additional domain-specific constraints, investigate its application to other areas with tailored domain constraints, and examine its potential for RUL prediction. This approach could also be extended to handle more complex degradation scenarios, building on the methodology presented here. Overall, this research offers a promising direction for future prognostic applications, improving the reliability and effectiveness of asset health management strategies.

## REFERENCES

- Biggio, L., & Kastanis, I. (2020). Prognostics and health management of industrial assets: Current progress and road ahead. *Frontiers in Artificial Intelligence*, 3, 578613.
- Blondel, M., Teboul, O., Berthet, Q., & Djolonga, J. (2020). Fast differentiable sorting and ranking. *37th International Conference on Machine Learning, ICML 2020, Part F16814*, 927–936.
- Brkovic, A., Gajic, D., Gligorijevic, J., Savic-Gajic, I., Georgieva, O., & Di Gennaro, S. (2017). Early fault detection and diagnosis in bearings for more efficient operation of rotating machinery. *Energy*, 136, 63–71.
- Carino, J. A., Zurita, D., Delgado, M., Ortega, J. A., & Romero-Troncoso, R. J. (2015). Remaining useful life estimation of ball bearings by means of monotonic score calibration. *Proceedings of the IEEE International Conference on Industrial Technology, 2015-June*, 1752–1758.
- Chen, J., & Liu, Y. (2021). Probabilistic physics-guided machine learning for fatigue data analysis. *Expert Systems with Applications*, 168, 114316.
- Cleveland, W. S., & Devlin, S. J. (1988). Locally weighted regression: An approach to regression analysis by local fitting. *Journal of the American Statistical Association*, 83(403), 596–610.
- Cubillo, A., Perinpanayagam, S., & Esperon-Miguez, M. (2016). A review of physics-based models in prognostics: Application to gears and bearings of rotating machinery. *Advances in Mechanical Engineering*, 8(8), 1687814016664660.
- Duong, B. P., Khan, S. A., Shon, D., Im, K., Park, J., Lim, D. S., ... Kim, J. M. (2018). A reliable health indicator for fault prognosis of bearings. *Sensors (Switzerland)*, 18(11).
- Hoffmann Souza, M. L., da Costa, C. A., & de Oliveira Ramos, G. (2023). A machine-learning based data-oriented pipeline for Prognosis and Health Management Systems. *Computers in Industry*, 148(January), 103903.
- Jieyang, P., Kimmig, A., Dongkun, W., Niu, Z., Zhi, F., Jiahai, W., ... Ovtcharova, J. (2023). A systematic review of data-driven approaches to fault diagnosis and early warning. *Journal of Intelligent Manufacturing*, 34(8), 3277–3304.
- Karniadakis, G. E., Kevrekidis, I. G., Lu, L., Perdikaris, P., Wang, S., & Yang, L. (2021). Physics-informed machine learning. *Nature Reviews Physics*, 3(6), 422–440.
- Lei, Y., Li, N., Gontarz, S., Lin, J., Radkowski, S., & Dybala, J. (2016). A model-based method for remaining useful life prediction of machinery. *IEEE Transactions on Reliability*, 65(3), 1314–1326.
- Lei, Y., Li, N., Guo, L., Li, N., Yan, T., & Lin, J. (2018). Machinery health prognostics: A systematic review from data acquisition to RUL prediction. *Mechanical Systems and Signal Processing*, 104, 799–834.

Bearings	Soft Rank CCAE based HI Estimation			CCAe based HI Estimation		
	Trendability	Robustness	Consistency	Trendability	Robustness	Consistency
Bearing_1.1	-0.972 ± 0.009	0.754 ± 0.025	<b>0.986 ± 0.008</b>	<b>-0.991 ± 0.005</b>	<b>0.946 ± 0.003</b>	0.921 ± 0.070
Bearing_1.2	<b>-0.970 ± 0.003</b>	0.744 ± 0.014	<b>0.932 ± 0.066</b>	-0.963 ± 0.019	<b>0.941 ± 0.005</b>	0.723 ± 0.244
Bearing_1.3	<b>-0.893 ± 0.066</b>	0.769 ± 0.080	0.828 ± 0.121	-0.392 ± 0.394	<b>0.946 ± 0.016</b>	<b>0.856 ± 0.091</b>
Bearing_1.4	<b>-0.905 ± 0.035</b>	0.869 ± 0.032	<b>0.840 ± 0.118</b>	-0.785 ± 0.109	<b>0.948 ± 0.016</b>	0.814 ± 0.147
Bearing_1.5	<b>-0.093 ± 0.254</b>	0.816 ± 0.061	0.882 ± 0.115	0.316 ± 0.247	<b>0.946 ± 0.006</b>	<b>0.922 ± 0.073</b>
Bearing_1.6	<b>-0.077 ± 0.192</b>	0.775 ± 0.126	0.778 ± 0.210	0.157 ± 0.227	<b>0.922 ± 0.009</b>	<b>0.938 ± 0.059</b>
Bearing_1.7	<b>-0.552 ± 0.146</b>	0.883 ± 0.029	0.843 ± 0.138	0.339 ± 0.248	<b>0.948 ± 0.004</b>	<b>0.949 ± 0.046</b>
Bearing_2.1	-0.963 ± 0.005	0.700 ± 0.007	<b>0.976 ± 0.024</b>	<b>-0.983 ± 0.000</b>	<b>0.943 ± 0.004</b>	0.922 ± 0.070
Bearing_2.2	-0.970 ± 0.005	0.721 ± 0.016	<b>0.978 ± 0.020</b>	<b>-0.981 ± 0.001</b>	<b>0.949 ± 0.006</b>	0.959 ± 0.040
Bearing_2.3	<b>-0.403 ± 0.209</b>	0.749 ± 0.195	0.679 ± 0.200	-0.092 ± 0.337	<b>0.879 ± 0.091</b>	<b>0.743 ± 0.184</b>
Bearing_2.4	<b>-0.874 ± 0.051</b>	0.801 ± 0.063	0.751 ± 0.266	-0.665 ± 0.143	<b>0.930 ± 0.008</b>	<b>0.937 ± 0.066</b>
Bearing_2.5	<b>-0.273 ± 0.330</b>	0.637 ± 0.143	0.819 ± 0.132	-0.054 ± 0.488	<b>0.874 ± 0.037</b>	<b>0.896 ± 0.082</b>
Bearing_2.6	<b>-0.408 ± 0.251</b>	0.785 ± 0.083	0.885 ± 0.146	-0.220 ± 0.462	<b>0.917 ± 0.009</b>	<b>0.907 ± 0.083</b>
Bearing_2.7	<b>-0.765 ± 0.083</b>	0.776 ± 0.105	0.310 ± 0.353	-0.506 ± 0.320	<b>0.879 ± 0.107</b>	<b>0.600 ± 0.365</b>
Bearing_3.1	<b>-0.967 ± 0.004</b>	0.751 ± 0.016	0.937 ± 0.054	-0.947 ± 0.009	<b>0.938 ± 0.005</b>	<b>0.946 ± 0.057</b>
Bearing_3.2	<b>-0.964 ± 0.007</b>	0.688 ± 0.023	<b>0.984 ± 0.013</b>	-0.955 ± 0.008	<b>0.943 ± 0.004</b>	0.956 ± 0.045
Bearing_3.3	<b>-0.908 ± 0.028</b>	0.690 ± 0.052	0.837 ± 0.118	-0.599 ± 0.127	<b>0.918 ± 0.013</b>	<b>0.852 ± 0.143</b>

Table 6. Soft Rank CCAE Vs. CCAE based performance evaluations on all bearings.

- Li, H., Zhang, Z., Li, T., & Si, X. (2024). A review on physics-informed data-driven remaining useful life prediction: Challenges and opportunities. *Mechanical Systems and Signal Processing*, 209(December 2023), 111-120.
- Liao, L., & Kötting, F. (2014). Review of hybrid prognostics approaches for remaining useful life prediction of engineered systems, and an application to battery life prediction. *IEEE Transactions on Reliability*, 63(1), 191-207.
- Lu, W., Wang, Y., Zhang, M., & Gu, J. (2024). Physics guided neural network: Remaining useful life prediction of rolling bearings using long short-term memory network through dynamic weighting of degradation process. *Engineering Applications of Artificial Intelligence*, 127(PB), 107350.
- Meire, M., Brijder, R., Dekkers, G., & Karsmakers, P. (2022). Accelerometer-Based Bearing Condition Indicator Estimation Using Supervised Adaptive DSVDD. *Proceedings of the Annual Conference of the Prognostics and Health Management Society, PHM*, 14(1), 1-10.
- Meng, C., Seo, S., Cao, D., Griesemer, S., & Liu, Y. (2022). When physics meets machine learning: A survey of physics-informed machine learning. *arXiv preprint arXiv:2203.16797*.
- Mosallam, A., Medjaher, K., & Zerhouni, N. (2016). Data-driven prognostic method based on bayesian approaches for direct remaining useful life prediction. *Journal of Intelligent Manufacturing*, 27, 1037-1048.
- Muralidhar, N., Islam, M. R., Marwah, M., Karpatne, A., & Ramakrishnan, N. (2018). Incorporating Prior Domain Knowledge into Deep Neural Networks. *Proceedings - 2018 IEEE International Conference on Big Data, Big Data 2018*, 36-45.
- Nascimento, R. G., & Viana, F. A. (2019). Fleet prognosis with physics-informed recurrent neural networks. *Structural Health Monitoring 2019: Enabling Intelligent Life-Cycle Health Management for Industry Internet of Things (IIOT) - Proceedings of the 12th International Workshop on Structural Health Monitoring*, 2, 1740-1747.
- Patrick Nectoux, K. M., Rafael Gouriveau, Ramasso, E., & Brigitte Chebel-Morello, e. a. (2012). PRONOSTIA: An Experimental Platform for Bearings Accelerated Degradation Tests. *IEEE International Conference on Prognostics and Health Management, PHM'12., Jun 2012, Denver, Colorado, United States.*, 1-8.
- Raissi, M., Perdikaris, P., & Karniadakis, G. E. (2019). Physics-informed neural networks: A deep learning framework for solving forward and inverse problems involving nonlinear partial differential equations. *Journal of Computational Physics*, 378, 686-707.
- Rezaeianjouybari, B., & Shang, Y. (2020). Deep learning for prognostics and health management: State of the art, challenges, and opportunities. *Measurement: Journal of the International Measurement Confederation*, 163, 107929.
- Van Baelen, Q., & Karsmakers, P. (2023). Constraint guided gradient descent: Training with inequality constraints with applications in regression and semantic segmentation. *Neurocomputing*, 556, 126636.
- Vincent, P., Larochelle, H., Lajoie, I., Bengio, Y., Manzagol, P.-A., & Bottou, L. (2010). Stacked denoising autoencoders: Learning useful representations in a deep network with a local denoising criterion. *Journal of machine learning research*, 11(12).

- Vishwakarma, M., Purohit, R., Harshlata, V., & Rajput, P. (2017). Vibration Analysis & Condition Monitoring for Rotating Machines: A Review. *Materials Today: Proceedings*, 4(2), 2659–2664.
- Von Rueden, L., Mayer, S., Beckh, K., Georgiev, B., Gieselbach, S., Heese, R., ... Schuecker, J. (2023). Informed Machine Learning - A Taxonomy and Survey of Integrating Prior Knowledge into Learning Systems. *IEEE Transactions on Knowledge and Data Engineering*, 35(1), 614–633.
- Wang, J., Li, Y., Zhao, R., & Gao, R. X. (2020). Physics guided neural network for machining tool wear prediction. *Journal of Manufacturing Systems*, 57(October), 298–310.
- Willard, J., Jia, X., Xu, S., Steinbach, M., & Kumar, V. (2022). Integrating Scientific Knowledge with Machine Learning for Engineering and Environmental Systems. *ACM Computing Surveys*, 55(4), 1–34.
- Xiong, J., Fink, O., Zhou, J., & Ma, Y. (2023). Controlled physics-informed data generation for deep learning-based remaining useful life prediction under unseen operation conditions. *Mechanical Systems and Signal Processing*, 197.
- Xu, Y., Kohtz, S., Boakye, J., Gardoni, P., & Wang, P. (2023). Physics-informed machine learning for reliability and systems safety applications: State of the art and challenges. *Reliability Engineering & System Safety*, 230, 108900.
- Zhang, B., Zhang, L., & Xu, J. (2016). Degradation Feature Selection for Remaining Useful Life Prediction of Rolling Element Bearings. *Quality and Reliability Engineering International*, 32(2), 547–554.
- Zhou, H., Huang, X., Wen, G., Lei, Z., Dong, S., Zhang, P., & Chen, X. (2022). Construction of health indicators for condition monitoring of rotating machinery: A review of the research. *Expert Systems with Applications*, 203(March), 117297.